2000

Modeling the Raven SCS-700 Chemical Injection System with Carrier Control with Sprayer Simulation

Brian L. Steward
Iowa State University, bsteward@iastate.edu

Dan S. Humbrug
South Dakota State University

MODELING THE RAVEN SCS-700 CHEMICAL INJECTION SYSTEM WITH CARRIER CONTROL WITH SPRAYER SIMULATION

B. L. Steward, D. S. Humburg

ABSTRACT. *Mathematical models of the chemical and carrier control sub-systems of the Raven SCS-700 chemical injection system were developed. The step responses of both control sub-systems were predictable using the models. From this process of model development, it was observed that the voltage saturation effect limited the response speed of the carrier valve motor and the resulting speed at which changes could be made to the carrier flow rate. The rate at which flow rate measurements were available limited the extent to which valve motor speed could be increased without causing instability. The performance of three different types of sprayers was simulated using these models. Simulations were performed with and without carrier control. Sprayers using carrier control misapplied to smaller areas than those without carrier control. Differences between the response of the chemical and carrier sub-system controllers produced concentration variations that contributed to application error. These errors, however, were small relative to the errors caused by response times of both systems and the ground speed sampling rate.*
Keywords. *Chemical application, Dynamic model development, Flow control, Simulation.*

Large amounts of pesticides are applied each year to the fields of U.S. farmers. In 1995, about 939 million pounds of pesticides were used in agriculture (Aspelin, 1997). In 1997, $8.8 billion was spent on pesticides which represents a 3.5% increase over the $8.5 billion expenditure level of 1996. Herbicides account for 65 to 70% of these pesticides (Economic Research Service, 1997, 1998). Hence, herbicides represent a costly input to field crop production and are a source of environmental concern, yet they are relied on heavily for effective weed control to minimize yield loss in crop production.

Concerns over environmental degradation from misapplied chemicals have resulted in scrutiny of the methods and equipment used to apply these materials. Evidence exists that much pesticide may be applied at erroneous rates. While the USDA (1989) recommends that application error should not exceed 5% of the recommended rate, a number of researchers have found that in practice, errors commonly exceed this tolerance (Rider and Dickey, 1982; Ozkan, 1987; Grisso et al., 1988).

The finding of such errors has led to the development of electronic control systems as a method of reducing application errors and undesired variation in application rates. Direct chemical injection is an electronically controlled system in which a pesticide is injected into a carrier (Gebhardt et al., 1974; Vidrine et al., 1975; Reichard and Ladd, 1983; Larson et al., 1982; Peck and Roth, 1975). This type of system not only has the capability of reducing much of the error associated with variation in application vehicle ground speed, but also has other performance advantages, such as possible safety and environmental advantages.

Several studies characterized direct injection systems (Budwig et al., 1988; Tompkins et al., 1990; Sudduth et al., 1995). These studies found the principal limitation of chemical injection systems without carrier control to be the transport delay from the injection point to the application nozzles. Koo et al. (1987) developed a simulation to estimate application errors due to time delays. Additionally, Way et al. (1992) developed a simulation to predict formulation deposit rates of three types of direct boom injection sprayers that did not use carrier control. All of the simulated sprayers used a constant carrier flow rate and varied the chemical concentration proportionally with the ground speed. As a result, they produced an error in the application rate during changes in ground speed because of the transport delay in the plumbing from the injection point to the nozzle. Sudduth et al. (1995) studied the dynamic response of a Raven SCS-700 system without carrier control for use as a variable rate applicator. Transport delays also dominated errors in this system.

Carrier control has been added to some chemical injection systems in an effort to eliminate the problem of transport delay of chemical rate changes through the system plumbing. In a carrier controlled system, the rates of chemical and carrier are both changed in response to a change in speed or target rate. Perfect performance would imply a constant concentration of the chemical/carrier mix in the system plumbing with variation in the applied volume of this mix accounting for rate changes (Karsky et

Article has been reviewed and approved for publication by the Power & Machinery Division of ASAE.

Journal Paper J-18763 of the Iowa Agriculture and Home Economics Experiment Station, Ames, Iowa, Project No. 3506, and supported by Hatch Act and State of Iowa funds. The use of trade names is only meant to provide specific information to the reader and does not constitute endorsement by South Dakota State University or Iowa State University.

The authors are **Brian L. Steward**, ***ASAE Member Engineer***, Assistant Professor, Agricultural and Biosystems Engineering Department, Iowa State University, Ames, Iowa, and **Dan S. Humburg**, ***ASAE Member Engineer***, Associate Professor, Agricultural and Biosystems Engineering Department, South Dakota State University, Brookings, S.D. **Corresponding author:** Brian L. Steward, Iowa State University, 206 Davidson Hall, Ames, IA 50011, phone: 515.294.1452, fax: 515.294.2255, e-mail: <bsteward@iastate.edu>.

al., 1990). However, in real systems, dynamic differences in the chemical and control subsystems will generate transient concentration during changes in flow rates. The interaction of these dynamic differences is not well understood. As these systems are adapted to variable rate application, and for considerations of application accuracy and safety, it is important that the performance of the control systems for chemical and carrier metering be well understood in the context of the sprayers that they control. Characterization of the Raven SCS-700 injection system without carrier control has been accomplished (Budwig et al. 1988; Sudduth et al. 1995). However, no systematic evaluation or modeling has been reported on chemical injection systems with carrier control.

The addition of deliberately varied rates for precision agriculture applications increases the importance of understanding control system response and the interaction between chemical and carrier control subsystems. As a result, a study was undertaken to mathematically model a chemical injection system with carrier control and to apply these models in performance simulation of three types of prototypical sprayers.

OBJECTIVES

The objectives of this work were to:

1. Model mathematically the chemical control subsystem of the Raven Industries SCS-700 chemical injection system and design an appropriate controller.
2. Model mathematically the carrier control subsystem of the same system.
3. Simulate the performance of three types of sprayers using the subsystem models with and without carrier control and under different control system modifications.
4. Identify and characterize the limiting components and variables of this control system for chemical application.

METHODS AND MATERIALS

The Raven SCS-700 (Raven Industries, Inc., Sioux Falls, S.Dak.) chemical injection system was modeled in this study (fig. 1). Physical parameters needed for the models were determined for the sensors and actuators by which the chemical and carrier flow rates are physically changed. These parameters were determined from the manufacturers' data or experimentally. The Raven controller was not used, but new controllers were either designed or proposed and were included in the model. The chemical injection system consisted of both carrier and chemical control subsystems. Each subsystem was treated separately under the assumption that they could be considered to be uncoupled dynamically. This assumption was verified experimentally.

CHEMICAL CONTROL SUBSYSTEM MODELING

The chemical control subsystem consisted of a variable stroke (manually adjustable) positive displacement piston pump (Raven Industries Inc., Sioux Falls, S.Dak.) which was used to inject the chemical into the carrier. The shaft speed of the pump was used to determine the flow rate of chemical into the carrier since the chemical flow rate is proportional to the shaft speed. The pump was powered with a DC permanent magnet motor (Model Number 5075-005, Stature Electric, Inc., Watertown, N.Y.) which was coupled to the pump through a timing belt and pulley arrangement. The motor parameters were determined from the manufacturer's data. The pump was modeled as a variable load torque on the motor which was linearly related to the shaft speed of the pump and the outlet pressure of the pump. It was assumed the load torque component produced by the pump due to inertia was negligible compared with that due to friction. To determine this relationship, a test apparatus was built which allowed the motor and pump assembly to be operated at different speeds by varying the armature voltage of the motor (fig. 2). The pump outlet pressure was set with a pressure

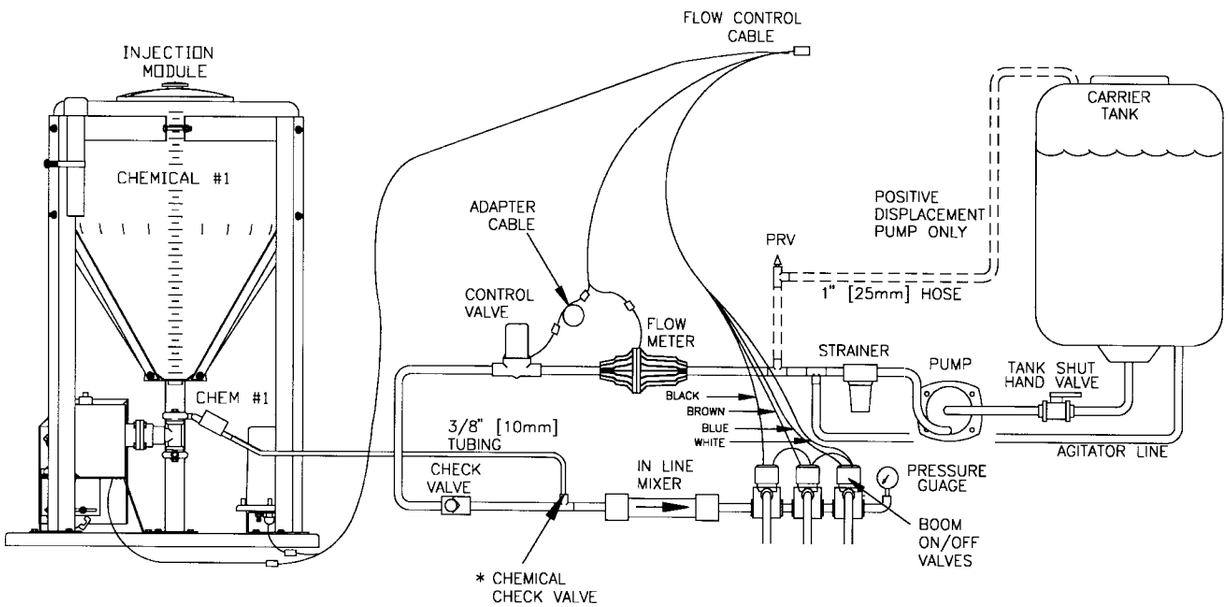

Figure 1–Illustration of the Raven SCS-700 chemical injection system with carrier control (Raven, 1987).

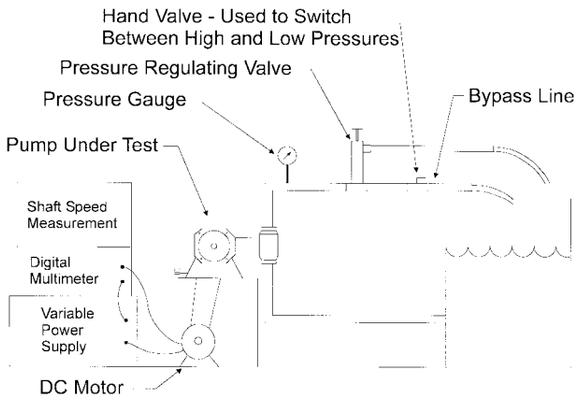

Figure 2–Chemical control subsystem test apparatus. The pressure regulating valve was used to create a pressure head at the pump outlet.

relief valve, and the pressure was measured with a pressure gauge. The pump speed was measured with a Hall effect sensor and shaft-mounted magnet. The pump speed was varied from 100 to 1700 rpm at six different outlet pressures (0, 172, 345, 517, 689 kPa). The armature voltage and current were measured for each condition and used along with the motor parameters to calculate load torque. No interaction effects between shaft speed and outlet pressure on load torque were observed. Linear regression was used to estimate slope of the torque-speed curve. The relationship between torque and pressure was estimated in a similar manner.

Two sensors provided feedback to the controller. A small dc motor (Model No. FYQM-63400-51, Barber-Colman Co., Rockford, Ill.) was used as a tachometer to measure the speed of the pump. This dc motor was coupled to the pump shaft with a small belt and pulley arrangement. The value of the tachometer's voltage constant was determined using a linear regression of empirical data. The shaft of the tachometer was turned at nine different speeds, and the armature voltage was measured at each speed. For the tachometer model, it was assumed that the tachometer voltage was strictly proportional to speed since the time constants associated with the tachometer were small in comparison to the motor, and therefore, all energy storage effects in the tachometer were considered to be negligible. In addition, a gear tooth sensor (Model Number 1GT101DC, Micro Switch Inc., Minneapolis, Minn.), which produced a voltage square wave as a 27-tooth gear mounted on the pump shaft passed by it, served as a digital pump shaft position sensor.

Chemical Control Subsystem Controller Development

A novel phase-locked loop (Geiger, 1981) proportional-integral (PI) controller was developed and tested for use with the chemical injection system. The command signal sent into the controller was a square wave whose frequency corresponded to that produced by the gear tooth sensor for the desired pump shaft speed. This control signal clocked the "UP" count pin of a four-bit digital counter while the digital feedback signal clocked the "DOWN" count pin of the same counter. This counter was connected in cascade with another identical counter, and the eight-bit output of the two counters were converted to a voltage level through a digital-to-analog converter (DAC). The counters were integrators functionally since if there was a frequency difference between the command and feedback signals, the counters would start incrementing (or decrementing) and thus integrate the error. When the two frequencies were matched, the count toggled between two values as increment transitions and decrement transitions were received. The dc average of the signal was thus a function of the phase difference between the two signals, and the controller tended therefore to drive the system to a phase-lock condition between these two signals. The proportional feedback signal generated by the tachometer was subtracted from the analog signal from the DAC by using a differential amplifier. The tachometer signal was filtered by a passive low pass filter with a 10.8 Hz bandwidth to eliminate the effects of commutation noise in the signal.

To change the chemical flow rate, the speed of the pump and dc motor was changed by varying the armature voltage of the dc motor with a pulse-width-modulated (PWM) signal. This was accomplished by using a field-effect transistor (FET) bridge circuit which was driven by a PWM control integrated circuit. This circuit varied the duty cycle of a 6 kHz square wave which was supplied to the gates of the FET bridge according to level of analog signal produced by the differential amplifier. This controller was fully implemented in hardware and included in the chemical control subsystem model.

Model Verification

A block diagram description of the chemical control subsystem plant and controller model was developed (fig. 3). While there was a digital element to the controller in the digital counters, the quantization effects were considered to be negligible, and the chemical subsystem was modeled with a continuous-time model. Analytically, the block diagram was reduced to a transfer function, and the poles of the systems were determined. Using MATLAB (The MathWorks, Inc., Natick, Mass.), the step response of the sub-system was simulated. Experimentally, the controller was given a step command input corresponding to a pump shaft speed of 260 rpm to 990 rpm and from 990 rpm to 260 rpm. The rise and fall times corresponding to these step inputs were measured as the outlet pressure was varied from 0 to 1.24 MPa (0 to180 psi).

Carrier Control Subsystem Modeling: Components

A hydraulic test system was assembled which simulated a hydraulic system which might be encountered on a sprayer and would be controlled by the carrier controller. This test system consisted of a centrifugal pump (Series 9202C, Hypro Corp, New Brighton, Minn.), a 1-in. butterfly control valve (Model No. 445, Raven Industries), a flow meter (Model No. RFM55, Raven Industries), and five flow regulators (Part No. 4916-250, Spraying Systems Co. Wheaton, Ill.) to simulate nozzles. An AC electric motor was used as the prime mover to provide mechanical power to the pump, and the hydraulic components were plumbed with 1 1/4 in. rubber hose and with 3/4 in. hose making up the distribution plumbing where the flow regulators were mounted. The flow regulators were open to the atmosphere, and the water which was circulated through the system was sprayed into a 50 gallon tank

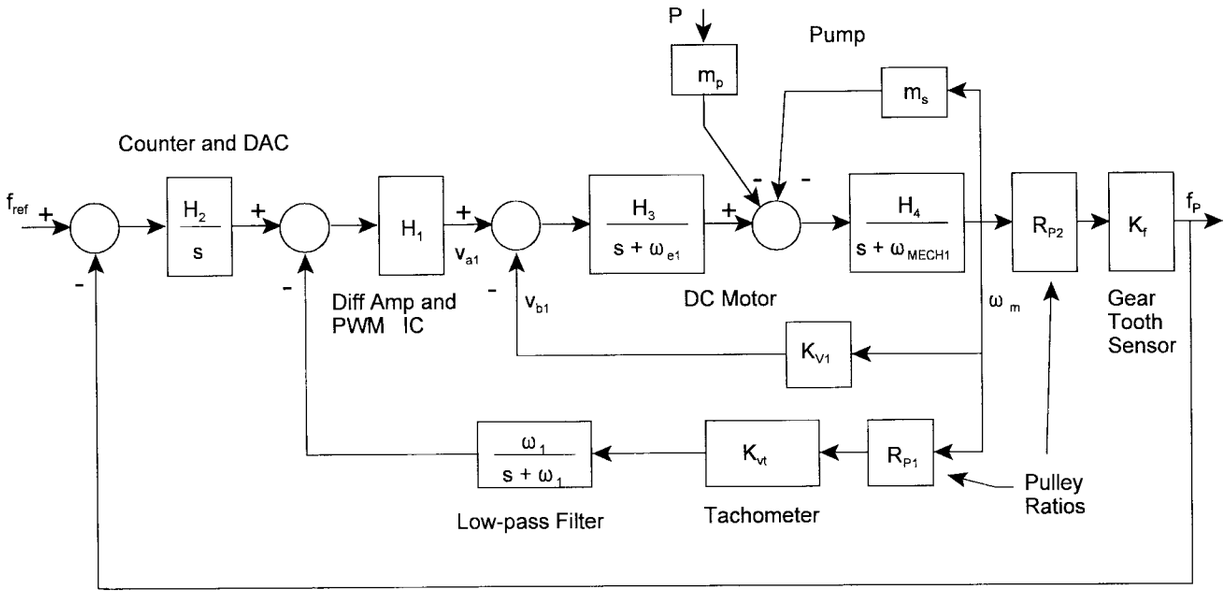

Figure 3–Chemical control subsystem block diagram.

which served as a system reservoir (fig. 4). The pressure-flow relationship for the hydraulic components was determined by using this test system. This was done by measuring the pressure drop across the components with pressure gauges and the corresponding flow rate with the system flow meter.

The pressure-flow characteristics of the hydraulic components (except the pump) were modeled as turbulent orifice flow as described by the equation:

$$Q = C_D A_0 \sqrt{\frac{2}{\rho} \Delta P} \qquad (1)$$

where ΔP is the pressure drop across the orifice, Q is the volumetric flow rate, C_D is the discharge coefficient for the orifice, A_0 is the area of the orifice, and ρ is the mass density of the fluid (Merritt, 1967). Solving for ΔP:

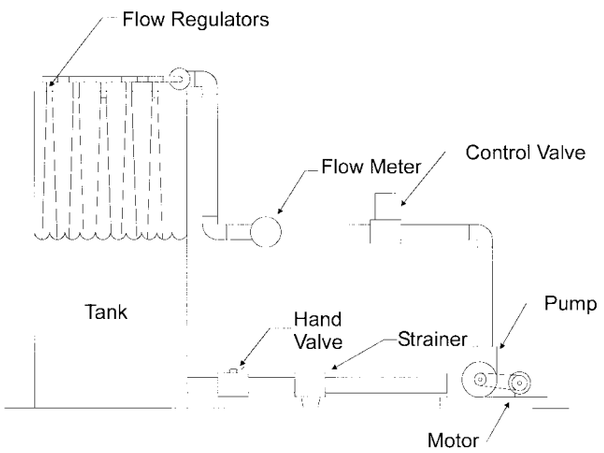

Figure 4–Carrier control subsystem test system.

$$\Delta P = K_Q Q^2 \qquad (2)$$

where $K_Q = 1/(2C_D^2 A_0^2)$ under the assumption that water is the carrier (ρ = 1 kg/L). Thus ΔP is proportional to the square of the flow rate and the flow characteristics of a particular component can be characterized by the value of K_Q, the pressure-flow coefficient for that component. The model development for the individual components is outlined below.

Flow Regulator Model. Since the flow regulators were orifices simulating spray nozzles, equation 2 naturally fit the pressure-flow data which were provided by the manufacturer and K_{QN} was easily determined by a least-squares fit of the data. K_{QN} captured the effect of the five flow regulators operating in parallel and was equal to the pressure-flow coefficient of an individual regulator divided by 5^2 since K_Q is inversely proportional to the square of the area.

Plumbing Model. The pressure-flow relationship in the plumbing was determined experimentally. Pressure was measured at the down-stream side of the control valve with a pressure gauge, and the difference between this measured value and that at the flow regulators as calculated from the manufacturer's specifications was determined for 10 different flow rates. These data were fit with equation 2 and K_{QP} was determined.

Flow Meter Model. The flow meter generated a square waveform having a frequency proportional to the flow rate of the fluid passing through it. The period of this waveform varied from 0.83 s to 0.015 s as the flow meter was calibrated to generate 72 pulses per 3.785 liters (1 gal) over a range of 3.785 to 208 L/min (1 to 55 gal/min). The period was the shortest possible time for the computer to acquire the most recent reading of the flow rate, and this time varied depending on the flow rate of the carrier. All sampling intervals, except for those associated with flow rates less than 15 L/min (4 gal/min), were less than 0.2 s.

Thus in the simulations, the sampling interval was assumed to be 0.2 s which would represent a worst case sampling interval for all flow rates greater than 15 L/min. The flow meter's pressure-flow characteristic provided by the manufacturer was used to determine K_{QFM} of the flow meter by fitting equation 2 to these data.

Valve Model. The control valve was modeled as an orifice with variable area and shape as a function of the valve element's angular position. The relationship between the pressure drop across the valve and the flow rate and position was determined experimentally. The pressure drop across the valve was measured with pressure gauges on the upstream and downstream sides of the valve while varying the flow rate of water through the valve with another control valve and varying the measured angle of the butterfly disc within the center of the valve body. Data were collected at nine different valve angles. For each valve angle position in these tests, a pressure-flow coefficient (K_{QV}) was calculated using a least-squares estimate. A third-order polynomial was used to fit the relationship between the natural logarithm of K_{QV} and valve angle in the least-squares sense (fig. 5). The exponential of both sides of this equation was taken to yield an equation for K_{QV} in terms of valve disk angle, θ:

$$K_{QV} = A \exp\left(c_3\theta^3 + c_2\theta^2 + c_1\theta\right) \qquad (3)$$

where

$A = 7.54 \times 10^{-4}$ kPa/(L/min)^2
$c_3 = -5.98447 \times 10^{-6}$ degrees^{-3}
$c_2 = 1.7727 \times 10^{-3}$ degrees^{-2}
$c_1 = -0.01418$ degrees^{-1} for the valve under test

A permanent magnet dc gear-motor (Model No. CYHC-43300, Barber-Colman Co.) was used to turn the valve stem of the control valve. The parameters describing this motor were determined from the manufacturer's data sheets.

Since the maximum voltage which could be applied to the valve motor was the system voltage (12 V), the output shaft speed was also limited. This limitation introduced a saturation nonlinearity to the system. To model the effects of voltage saturation, a voltage saturation transfer block was included in the model of the carrier control subsystem.

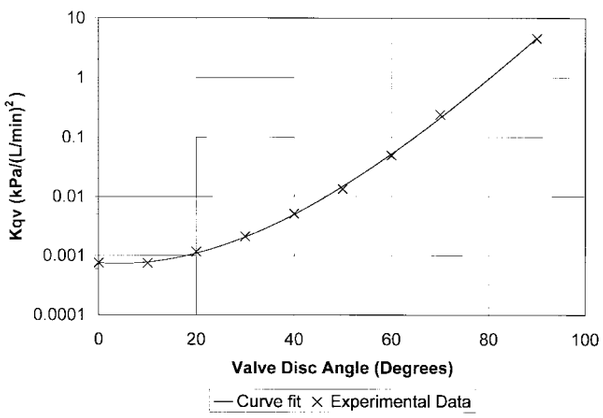

Figure 5–Control valve pressure-flow coefficient (K_{qv}) versus valve disc angle.

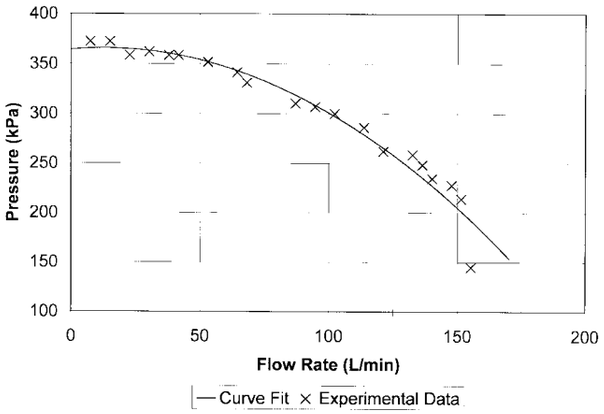

Figure 6–Pressure rise across the centrifugal pump as a function of the flow rate through the pump.

Centrifugal Pump Model. The relationship between the pressure rise across the centrifugal pump and the flow rate of the water being pumped was determined experimentally by measuring the pressure at the outlet of the pump with a pressure gauge at different flow rates (measured by the flow meter). By varying the angle of the control valve, pressure and flow measurements were taken at 20 different points. A second-order polynomial was fit to the experimental data by least-squares (fig. 6), and the equation describing this relationship was:

$$P_{PUMP} = a_2Q^2 + a_1Q + a_0 \qquad (4)$$

where

P_{PUMP} = pressure rise across the pump
Q = volumetric flow rate

For the pump under test:

a_2 = –0.0086 kPa/(L/min)^2
a_1 = 0.22 kPa/ (L/min)
a_0 = 364.4 kPa

Nonlinear Hydraulic Model. Considering the pressure-flow relationships of the various components described above and how they were interconnected, a model for the hydraulic section of the carrier control subsystem was developed. The block diagram of the hydraulic portion of the carrier subsystem was used as the basis for the nonlinear model of the carrier hydraulics (fig. 7). The hydraulic system model involved nonlinear second-order and third-order relationships between flow and pressure and provided a nonlinear transfer function between valve disc angle and flow rate.

Carrier Control Subsystem Controller Development

Although a variety of options were explored in the course of the work, a proportional feedback controller was ultimately included in the model for the carrier control subsystem. This sampled-data controller would sample carrier flow rate data from the flow meter at discrete points in time, calculate the desired reference or target flow rate,

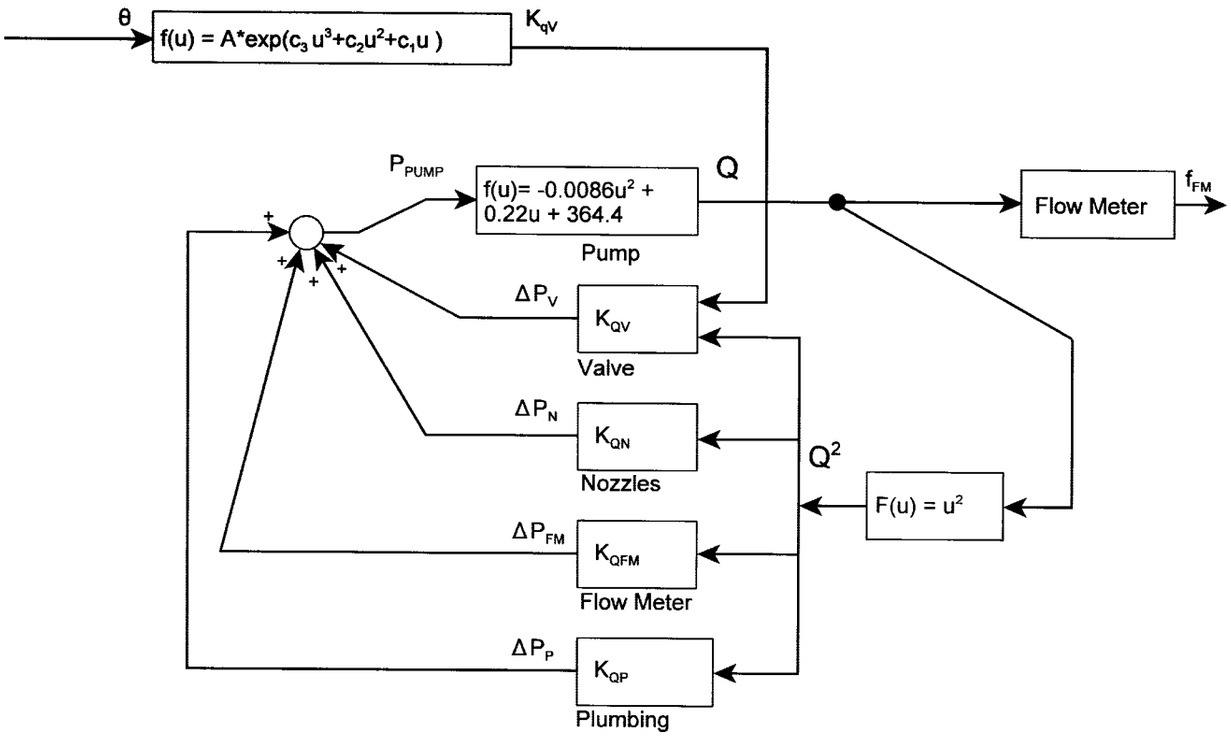

Figure 7–Carrier hydraulic model block diagram.

determine the error in the actual flow rate, and amplify the error signal by the controller gain. The resulting control signal would then be applied to the armature of the valve motor in a zero-order-hold fashion. This controller was not implemented in hardware, but it was used in the simulation of the system.

MODEL VERIFICATION

Non-linear Hydraulic Model. There was interest in verifying if the model adequately described the relationship between flow rate and valve angle. It was thus important to compare the flow rate as predicted by the model with that which was measured, both as a function of flow rate.

The flow rate for a particular valve disc angle was estimated by first solving for the pressure-flow coefficient (K_{QV}) of the valve associated with an angle using equation 3. Second, K_{QV} was substituted into an equation written in terms of flow rate. This equation was written based on a loop equation around the hydraulic circuit in terms of pressure. Mathematically, this equation was :

$$P_{PUMP} = \Delta P_V + \Delta P_N + \Delta P_{FM} + \Delta P_P \qquad (5)$$

where P_{PUMP} was the pressure rise across the pump, and ΔP_V, ΔP_N, ΔP_{FM}, and ΔP_P were the pressure drops across the valve, nozzles, flow meter, and plumbing, respectively. Substituting the flow relationships from the component models for pressure resulted in:

$$a_2Q^2 + a_1Q + a_0 =$$

$$\left[K_{QV}(\theta) + K_{QN} + K_{QFM} + K_{QP}\right] Q^2 \qquad (6)$$

where $K_{QV}(\theta)$, K_{QN}, K_{QFM}, K_{QP} are the pressure-flow coefficients for the valve, spray nozzles, flow meter, and plumbing, respectively.

This quadratic equation in the variable Q was solved by using the quadratic formula and taking the positive root. The carrier flow rate was determined over the range of valve disc angles from 0° to 90° using this formula. Experimentally, the flow rate was measured using the flow meter at nine different valve element angles using the hydraulic test system.

Overall Carrier Control Subsystem Model. A block diagram description of the carrier control subsystem and controller model was developed (fig. 8). For purposes of simulating the dynamic response of this subsystem, a state-space model was developed. A state-space model was used instead of a transfer function model because it was better able to model the effects of the subsystem's nonlinearities, and its step response was easily evaluated numerically by a computer program. Given the state-space model, the continuous-time model was transformed to a discrete-time model using the standard transformation involving the matrix exponential (Franklin et al., 1990) with a 0.2-s sampling time.

The step response of the modeled chemical sub-system with the proportional controller was calculated using Matlab for proportional gains of 20 and 40 and for steps from 18.9 L/min (5 gal/min) to 56.8 L/min (15 gal/min) and 18.9 L/min (5 gal/min) to 28.4 L/min (7.5 gal/min). The simulated step response of the proportional controller was compared with that of the Raven controller controlling the hydraulic test system in the laboratory. When the Raven controller was given a command step, it applied 12 V to the motor until the flow rate was measured to be within 10% of

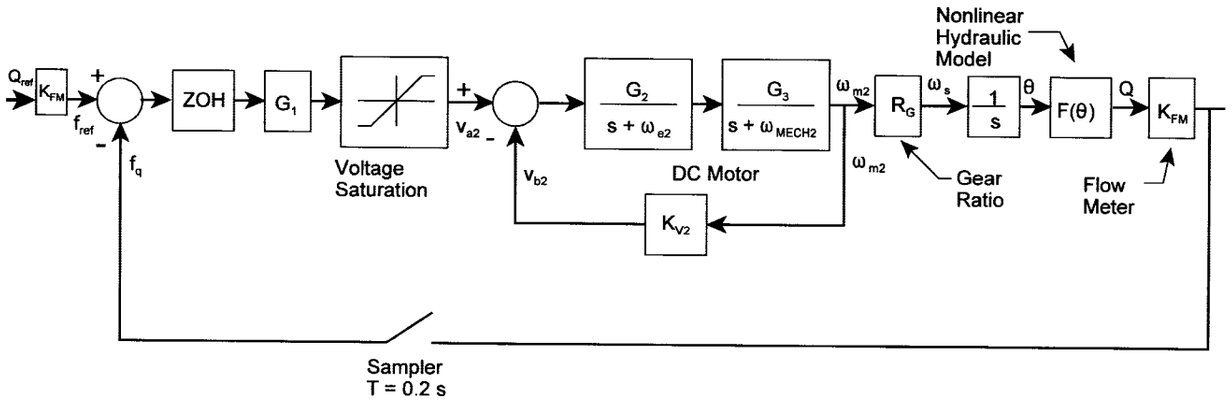

Figure 8–Carrier control subsystem block diagram where $G_2 = K_T/L_a$, $G_3 = 1/J_m$, $W_{e2} = R_a/L_a$, $W_{MECH2} = B_m/J_m$ are the motor electrical gain, mechanical gain, electrical pole frequency, and mechanical pole frequency, respectively.

the commanded flow rate at which point the voltage started being pulsed at the motor. The voltage applied to the valve motor was measured using a chart recorder (Model DASH IV, Astro-Med, Inc.,West Warwick, R.I.) to determine the rise or fall time required to respond to a step command. The Raven controller was commanded to change the flow rate of the carrier for five different step sizes. The step responses of the modeled system to these same step inputs were determined by simulation, and the rise and settling times were recorded for all cases.

SPRAYER SIMULATION

A computer program was written to simulate the performance of three types of sprayers (Steward, 1994). These sprayer configurations (private broadcast, commercial broadcast, and private band) were the same as given by Way et al. (1992) and differed only in their anticipated travel speed and physical plumbing and nozzle layout which came from the average dimensions of actual sprayers as measured in a survey of herbicide applicators (Grisso et al., 1988).

The first sections of the program initialized the simulation for the type of sprayer and controller design to be simulated. Next, a sequence of numbers was generated which simulated the vehicle ground speed sampled at every 0.1 s. The speed function consisted first of a ramp with a slope of 1.6 km/h/s (1 m/h/s) increasing from the initial intended field speed of the prototypical sprayer (Way et al., 1992) to the final speed which was a 30% increase over the initial speed. The speed was then held constant at that speed. The 30% change in speed corresponded to a 30% change in flow rate which was within the maximum change in flow rate that could occur while insuring that the spray nozzles still maintained a uniform spray pattern (Ayers et al., 1990; Spraying System Co., 1993). The acceleration was the maximum typical acceleration for agricultural vehicles according to Gebhardt et al. (1974).

Next, the program averaged the speed function over the controller's sampling time period and that average speed was used over the next sampling time period to calculate the commanded flow rate. When a change in speed was detected, the controller issued a step command to the subsystem controller, and the models were used to calculate the corresponding dynamic response. Once the chemical and carrier flow rates of the subsystems were calculated, the concentration of the chemical in the carrier could be calculated at the injection point. Though ideally constant, the injection concentration did vary because of the differences in the individual subsystem dynamics. The variations in concentration traveled to the nozzles arriving after a transport delay based on plumbing volume and flow rate. This transport delay time was different for each nozzle and was calculated in the next part of the program using the method described by Way et al. (1992).

Next, the formulation application rate at each nozzle was calculated. The concentration for this calculation was the nozzle concentration which was equal to the injection concentration at an earlier time, as it was assumed that there was no diffusion of the chemical in the carrier. The time difference was equal to the transport delay time.

The performance of the different types of sprayers was measured by summing the area of ground covered by a formulation application rate that was more than 5% from the desired application rate. The ratio of the area with an unacceptable application rate (i.e., outside of the ± 5% tolerance) to the total area sprayed in a distance of 402 m (0.250 mile) was calculated. This value, expressed as a percentage, was used as a measure of performance for a sprayer configuration during the period of acceleration.

Each of the three types of sprayers was simulated with several variations in the sprayer configuration. First, "baseline" simulations were performed which used carrier control with the carrier subsystem model with a proportional controller gain of 20 and a 0.9 rpm carrier valve motor. The ground speed was sampled every 0.5 s. Then, a set of simulations were run without carrier control. Next, two more sets of simulations were run with a similar sprayer configuration as the baseline simulations except with the sampling interval for the ground speed reduced, first to 0.3 s and then to 0.1 s. Then two sets of simulations were run with the same configuration as the baseline except that the maximum valve shaft speed was set at 1.8 rpm and 3.5 rpm. A final set of simulations was performed with the maximum valve shaft speed set at 1.8 rpm, the proportional controller gain set at 20, and the ground speed sampling rate set at 0.1 s.

Table 1. Chemical control subsystem parameter values as derived from the components of the test system

Parameter Name and Variable	Parameter Value
Differential amplifier and PWM IC Gain, H_1	7.34
Digital-to-analog conversion factor, H_2	0.04V/bit
Filter pole frequency, ω_1	68 rad/s
Motor to pump pulley ratio, R_{P2}	22/36
Motor to tachometer pulley ratio, R_{P1}	1.5
Motor back voltage constant, K_{V1}	0.0429 V/(rad/s)
Digital sensor conversion factor, K_f	$27/2\pi$ pulses/rad
Motor electrical gain, H_3	172.7 N-m/V-s
Motor electrical pole frequency, ω_{e1}	610 rad/s
Motor mechanical gain, H_4	5.10 (rad/s^2)/mN-m
Motor mechanical pole frequency, ω_{MECH1}	1.0 rad/s
Pump speed to torque transfer gain, m_s	1.34 mN-m/(rad/s)
Pump pressure to torque transfer gain, m_p	0.613 mN-m/kPa

RESULTS

CHEMICAL CONTROL SUBSYSTEM RESULTS

The parameters for the model were determined from the components which made up the test system (table 1). When the block diagram was reduced to a transfer function from command signal frequency to that proportional to the pump shaft speed, this transfer function was fourth-order with four poles with numerical values of –607, –36.9 ±j 179, and –2.28. The lone zero occurred at –68. These pole locations implied that the closed-loop system was stable and that the step response was dominated by the real pole at s = –2.28.

From simulation, a step response plot revealed that the sub-system had a 10 to 90% rise time of approximately 0.95 s. This was based on the subsystems dominant pole location The steady-state error was zero, as anticipated with integral control.

Experimentally, the system had a step response rise time of 0.9 s which was determined in the laboratory with step changes in the frequency of the input pulse train. The rise time was constant as the pressure head was varied from 0 to 1241 kPa (0 to 180 psi) and as the chemical metering pump stroke length setting was changed from the minimum to the maximum setting. It was concluded that the dynamics of the chemical control subsystem were adequately described by the model. Additionally, the controller design was robust to changes in the pump setting and the head pressure, both of which represent changes in the load torque on the dc motor. This finding provided evidence that the two subsystems could be considered dynamically uncoupled.

Table 2. Carrier control subsystem parameter values as derived from the components of the test system

Parameter Name and Variable	Parameter Value
Armature resistance, R_a	18.6 Ohms
Armature inductance, L_a	24.9 mH
Valve motor torque constant, K_T	98.3 mN-m/A
Valve motor back voltage constant, K_{V2}	0.0983 V/rad/s
Valve motor rotor moment of inertia, J_m	0.00925 mN-m-s^2
Valve motor damping constant, B_m	0.00847 mN-m-s
Valve motor gear ration, R_G	1/1263
Flow meter calibration constant, K_{FM}	0.322 Hz/(L/min)
Valve pressure-flow coefficient, K_{QV}*	7.5×10^{-4} to 4.6 kPa/(L/min)^2
Nozzles pressure-flow coefficient, K_{QN}	0.012 kPa/(L/min)^2
Plumbing pressure-flow coefficient, K_{QP}	0.022 kPa/(L/min)^2
Flow meter pressure-flow coef., K_{QPM}	0.0011 kPa/(L/min)^2

* Coefficient values for valve vary as a function of valve element angle.

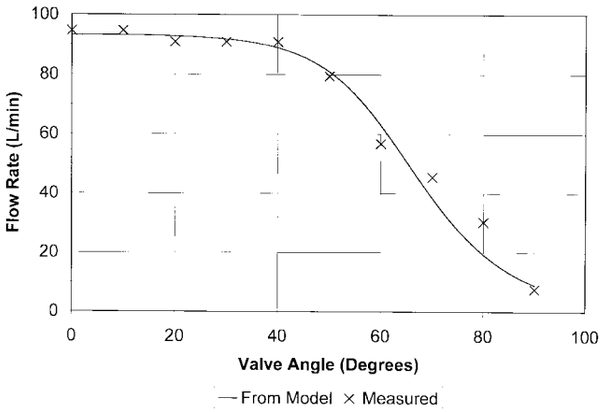

Figure 9–Variation in flow rate as a function of the valve element angle for the carrier test system.

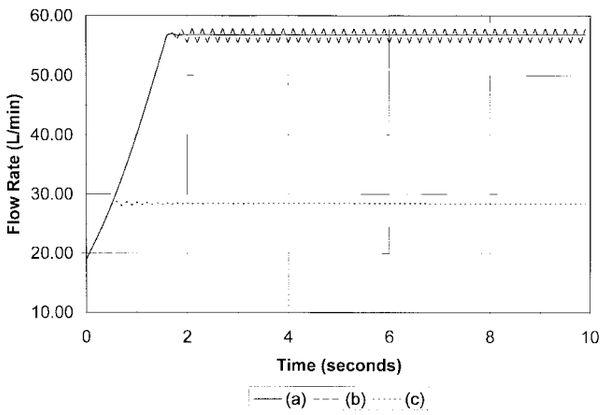

Figure 10–Simulated step response of the carrier subsystem and controller model for three cases: (a) step from 18.9 to 56.8 L/min with G_1 = 20; (b) step from 18.9 to 56.8 L/min with G_1 = 40; and (c) step from 18.9 to 28.4 L/min with G_1 = 40.

Table 3. Comparison of carrier controllers and valve motor speeds

	Proportional Controller (simulated)					
	Raven Controller (experimental data)		Max. Valve Speed = 0.91 rpm		Max. Valve Speed = 1.8 rpm	
Step Size L/min (gal/min)	Rise Time (s)	Settling Time (s)	Rise Time (s)	Settling Time (s)	Rise Time (s)	Settling Time (s)
92.7 to 75.7 (24.5 to 20.0)	4.4	4.7	4.0	1.0	2.0	1.0
75.7 to 37.9 (20.0 to 10.0)	3.2	0.0	2.8	0.4	1.4*	0.7*
37.9 to 75.7 (10.0 to 20.0)	2.5	2.85	2.8	0.7	1.6*	1.6*
37.9 to 18.9 (10.0 to 5.0)	1.9	6.0	1.8	1.0	0.75	0.75
18.9 to 37.9 (5.0 to 10.0)	1.3	0.0	1.75	0.5	0.75*	1.0*

* G_1 = 10.

CARRIER CONTROL SUBSYSTEM RESULTS

The state space description of the non-hydraulic part of the subsystem follows.

State equation:

$$\begin{bmatrix} \dot{x}_1 \\ \dot{x}_2 \\ \dot{x}_3 \end{bmatrix} = \begin{bmatrix} -\frac{R_a}{L_a} & \frac{K_{V2}}{L_a} & 0 \\ \frac{K_T}{J_m} & -\frac{B_m}{J_m} & 0 \\ 0 & R_G & 0 \end{bmatrix} \begin{bmatrix} x_1 \\ x_2 \\ x_3 \end{bmatrix} + \begin{bmatrix} \frac{1}{L_a} \\ 0 \\ 0 \end{bmatrix} v_{a2} \qquad (7)$$

Output equation:

$$Q = F(x_3) \qquad (8)$$

where the state variables: x_1 is the valve motor armature current as measured in amperes; x_2 is the valve motor rotor speed in unit of rad/s [denoted as ω_{m2} in the block diagram fig. 8)]; and x_3 is the valve disc angle in units of radian [denoted as θ in the block diagram (fig. 8)]. The variable v_{a2} is the voltage which is applied to the valve motor armature. The output equation is the nonlinear function relating the valve angle to the flow which was derived from equations 3 and 6. The control law was expressed as:

$$v_{a2} = G_1 K_{FM}(Q_{ref} - Q) \text{ ɜ } -12V \le v_{a2} \le 12V \qquad (9)$$

where G_1 is the gain of the proportional controller, Q is the measured carrier flow rate, and Q_{ref} is commanded reference carrier flow rate (in units of L/min). The constraints on v_{a2} modeled the voltage saturation. The model parameter were derived using the methodology described above (table 2). The hydraulic nonlinear model produced a relationship between valve angle and flow rate which was consistent with measured results (fig. 9).

From the simulated step responses of the proportional controller and modeled plant, a proportional controller gain G_1 = 20, and a step input from 18.9 L/min (5 gal/min) to 56.8 L/min (15 gal/min) yielded a step response with a rise time of about 2.5 s and a slight overshoot (fig. 10). The system was stable and had zero steady-state error. With the gain G_1 = 40, the step response had the same rise time as

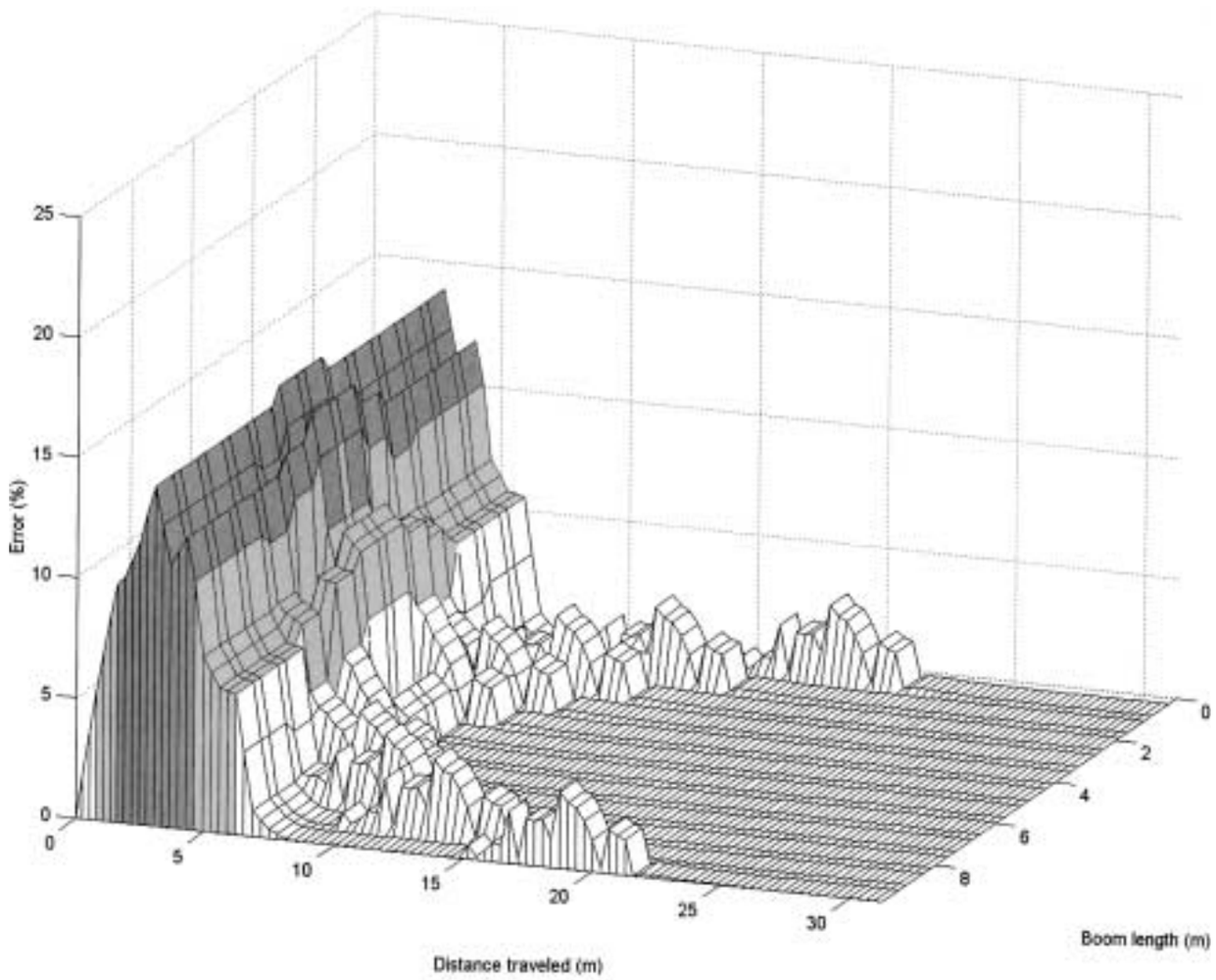

Figure 11–Application error versus distance traveled for the baseline simulation of the private broadcast sprayer with carrier control. White areas have less than 5% error. Gray areas have error between 5 and 10%. Dark gray areas have error greater than 10%.

the previous case, indicating that the control was saturated in both cases and the valve was turning at a maximum angular velocity (fig. 10). The rise time was fixed based on the angle through which the valve element had to turn to achieve the commanded change in flow rate. The oscillation on the response indicated that the system was unstable around this valve angle with $G_1 = 40$. However, with a smaller step from 18.9 L/min (5 gal/min) to 28.4 L/min (7.5 gal/min), the controller was stable with a gain, $G_1 = 40$ (fig. 10). Since the system was non-linear, it could not be characterized as globally stable or unstable. Stability depended on the size of the gain, G_1, and the operating point of the valve.

During the development of the model for the carrier subsystem plant, three hardware limitations were discovered all of which affected the performance of this subsystem. These limitations were: (1) the saturation effect of the limited system power supply which resulted in a maximum valve angular velocity; (2) the slow rate at which data was supplied from the flow meter; and (3) the nonlinear relationship between valve element angle, pressure, and flow rate.

There was little difference between the rise times of the Raven controller and the simulated proportional controller (table 3). Most of the rise time can be attributed to the period that the motor turned at saturation speed as it moved from one valve disc angle to another. The differences in rise time among the step sizes were due to the size of the angle though which the valve disc turned to achieve the commanded step. The settling time of the Raven controller was greater than that of the simulated proportional controller. This effect was a function of the algorithm. The Raven controller nudged the valve motor at a slow rate once the measured flow rate was within a small percentage of the commanded flow rate. This comparison showed the changes in the control algorithm did not change the rise time significantly, but algorithm changes could reduce the settling time.

Because of the similarity in the rise times between the simulation and the Raven controller, this comparison also provided validation for the simulation. Additionally, the comparison showed that the main limitation in developing a faster controller was the saturation that was manifested as the maximum valve angular velocity.

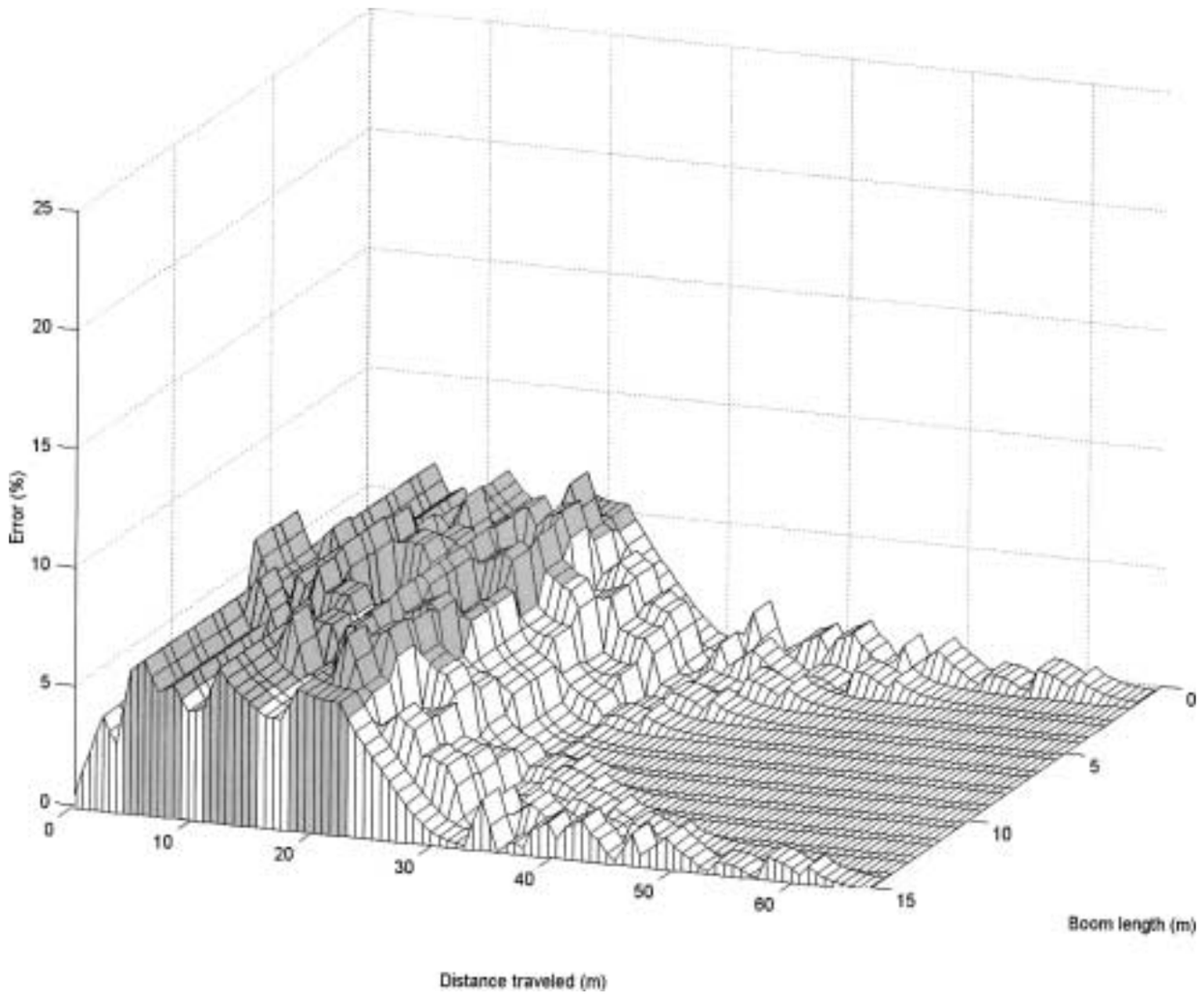

Figure 12–Application error versus distance traveled for the baseline simulation of the commercial broadcast sprayer with carrier control. White areas have less than 5% error. Gray areas have error between 5 and 10%. Dark gray areas have error greater than 10%.

Since the maximum speed of the valve motor appeared to be the limiting factor in reducing the rise time, operation of the proportional controller was simulated with the valve speed doubled. Doubling the speed of the motor reduced the rise time by approximately half (table 3). This result implied that a reduction of the rise time of the carrier flow rate could be accomplished by increasing the speed of the valve motor. The settling time did not change appreciably, however. In fact, in three of the cases where a 0.19 rad/s (1.8 rpm) valve motor was simulated, the system became unstable with proportional controller gain, G_1 = 20. To achieve stability, the controller gain was reduced to 10 for these three cases. It was observed that the valve motor speed could be increased to a point without introducing system instability, but further increases in motor speed would have to be accompanied by a decrease in controller gain or a reduction in the flow rate sampling time to reduce delay in the feedback loop.

SPRAYER SIMULATION RESULTS

From the baseline simulations, the plots of formulation application rate error as a function of distance showed the effects of the interaction of the response characteristics of the two control systems involved (figs. 11, 12, and 13). This interaction was most apparent in the plots for the private broadcast sprayer and the private banding sprayer (figs. 11 and 13). The large error at the beginning of the distance traveled was due to the delay produced by the slow sampling time and the delays in the response of ***both*** subsystems to the change in speed. The smaller peaks in error occurring after about 10 m of travel were due to concentration variation which was caused by differences in the response times ***between*** the chemical and carrier subsystems. The commercial broadcast sprayer went in and out of tolerance for some distance; the error peak was at about 5% with some variations around it (fig. 12). This error surface was different from that of the other two sprayers and was due to a longer acceleration distance for the commercial broadcast sprayer as compared with the other sprayers since it had a larger operating speed but still accelerated at the same rate.

For the baseline simulation, the percent of unacceptable area was the greatest for the broadcast sprayer used by commercial applicators at 4.02%. For the private applicator sprayers, the unacceptable area was 1.37% for the broadcast sprayer and 1.29% for the band sprayer (table 4).

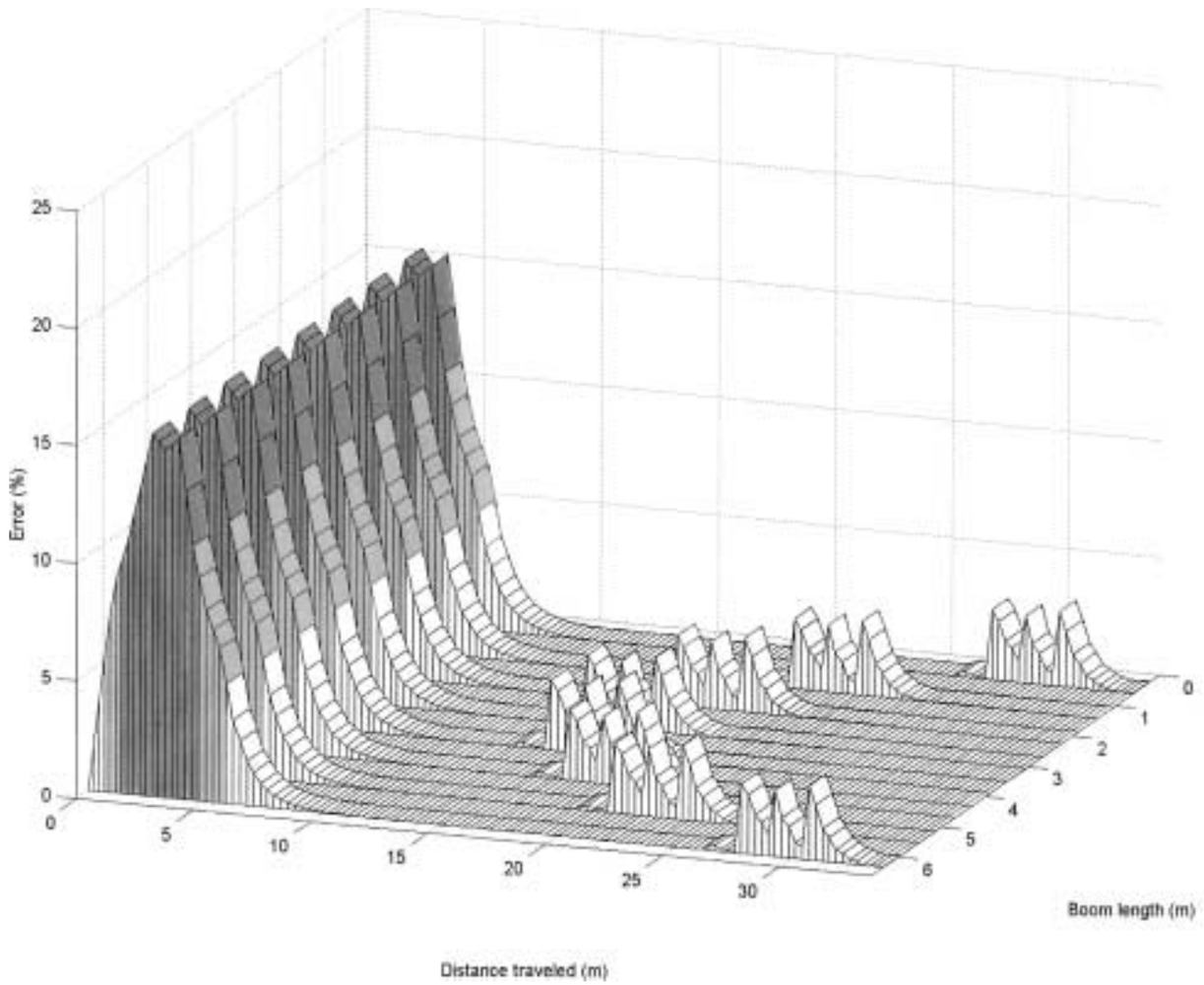

Figure 13–Application error versus distance traveled for the baseline simulation of the private band sprayer with carrier control. White areas have less than 5% error. Gray areas have error between 5 and 10%. Dark gray areas have error greater than 10%.

Table 4. Sprayer performance under variations of chemical and carrier control

Sprayer Type	Simulation Type	Unacceptable Area m^2 (ft^2)	Unacceptable Area (%)	Percent Change from Baseline
Private applicator Broadcast sprayer	Baseline simulation*	52.54 (565)	1.37	n/a
	No carrier control	102.8 (1,107)	2.69	+96
	Speed sampling rate = 0.3 s	42.9 (462)	1.12	–18
	Speed sampling rate = 0.1 s	24.6 (265)	0.64	–53
	Valve motor speed = 3.5 rpm	51.2 (551)	1.34	–2
	Valve motor speed = 1.8 rpm	52.1 (561)	1.36	–0.7
	Speed sampling rate = 0.1 s			
	Valve motor speed = 1.8 rpm	4.59 (49)	0.12	–91
Commercial applicator Broadcast sprayer	Baseline simulation*	240.6 (2,590)	4.02	n/a
	No carrier control	466.6 (5,022)	7.80	+94
	Speed sampling rate = 0.3 s	14.0 (150)	0.23	–94
	Speed sampling rate = 0.1 s	0	0.00	–100
	Valve motor speed = 3.5 rpm	153.5 (1,652)	2.56	–36
	Valve motor speed = 1.8 rpm	174.5 (1,879)	2.92	–27
	Speed sampling rate = 0.1 s			
	Valve motor speed = 1.8 rpm	10.2 (109)	0.17	–96
Private applicator band sprayer	Baseline simulation:*	15.8 (170)	1.29	n/a
	No carrier control	68.6 (739)	5.60	+334
	Speed sampling rate = 0.3 s	14.1 (151)	1.15	–11
	Speed sampling rate = 0.1 s	13.2 (142)	1.08	–17
	Valve motor speed = 3.5 rpm	12.3 (133)	1.00	–22
	Valve motor speed = 1.8 rpm	12.3 (133)	1.00	–22
	Speed sampling rate = 0.1 s			
	Valve motor speed = 1.8 rpm	9.67 (104)	0.79	–39

* The baseline simulation utilized Carrier Control, ground speed sampling rate of 0.5 s, and a valve motor speed of 0.9 rpm.

The simulated response of each sprayer without carrier control (figs. 14, 15, and 16) showed how the transport delays caused error in the formulation application rate until the new concentration arrived at the nozzles. For each sprayer type, the amount of unacceptable area for the simulation without carrier control was more than that of the simulation with carrier control. The percent of unacceptable area was 7.80% for the commercial applicator broadcast sprayer, 2.69% for the private applicator broadcast sprayer, and 5.60% for the private applicator band sprayer (table 4). Way et al. (1992) found the percent unacceptable area to be 8.9% for the commercial applicator broadcast sprayer, 2.7% for the private applicator broadcast sprayer, and 5.1% for the private applicator band sprayer. There was strong agreement between the results of this simulation and those of Way et al. (1992). The similarity in the results indicates that the transport delay of the chemical injection system without carrier control dominated other characteristics of the system since Way et al. (1992) did not consider delays due to ground speed sampling rate or controller dynamics which were included in this simulation.

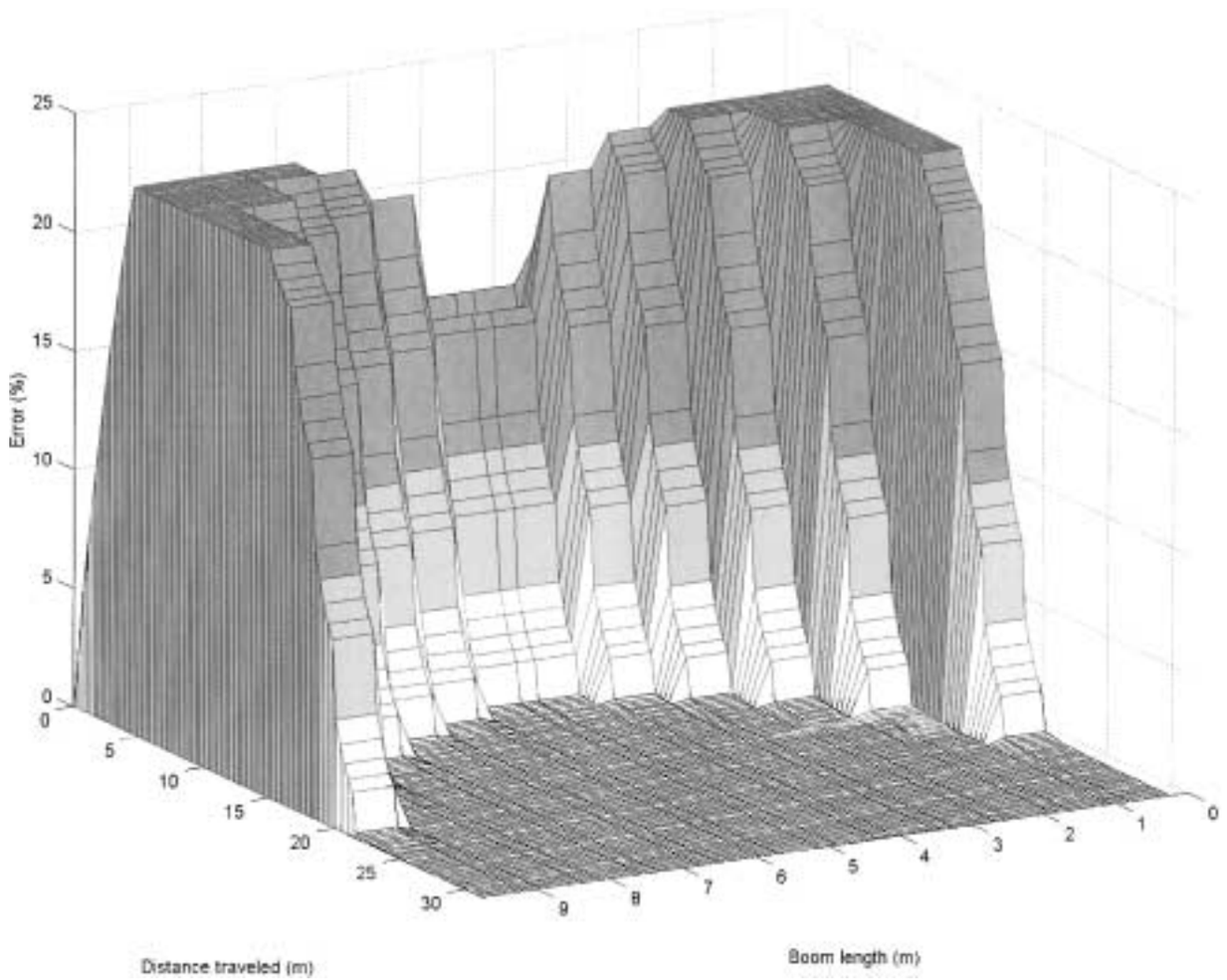

Figure 14–Application error versus distance traveled for the simulation of the private broadcast sprayer without carrier control. White areas have less than 5% error. Gray areas have error between 5 and 10%. Dark gray areas have error greater than 10%.

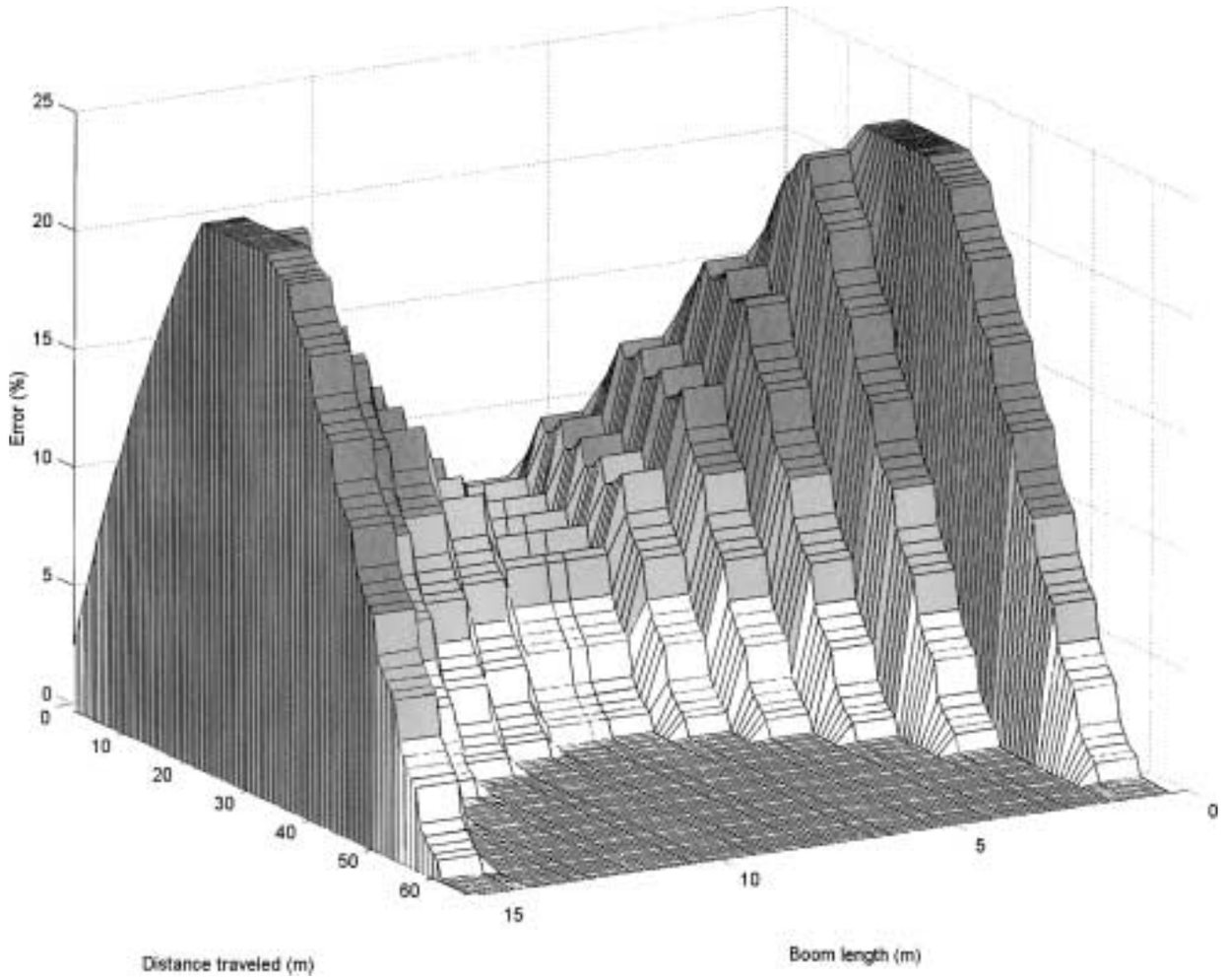

Figure 15–Application error versus distance traveled for the simulation of the commercial broadcast sprayer without carrier control. White areas have less than 5% error. Gray areas have error between 5 and 10%. Dark gray areas have error greater than 10%.

The simulations with the decreases in ground speed sampling interval showed corresponding decreases in area applied at a rate with more than 5% error. For the broadcast sprayer used by private applicators, the unacceptable area decreased from 1.37% in the baseline simulation to 1.12% for the 0.3 s sampling interval and to 0.64% for the 0.1 s interval. The broadcast sprayer used by commercial applicators also showed decreases in unacceptable area from 4.02% to 0.23% and 0.0%. The band sprayer had decreases in unacceptable area from 1.29% to 1.15% at the 0.3 s sampling rate and 1.08% at the 0.1 s sampling rate.

When simulations were run with the valve motor speed increased to 1.8 rpm, the unacceptable area decreased to 1.36% for the private broadcast sprayer, 2.92% for the commercial broadcast sprayer, and 1.00% for the private band sprayer. Increasing the valve motor speed to 3.5 rpm caused instability, so the gain of the proportional control was reduced to 10 to obtain the results listed. The unacceptable area decreased to 1.34% for the private broadcast sprayer, 2.56% for the commercial broadcast sprayer, and 1.00% for the private band sprayer for this change in motor speed. The final set of simulations with the valve motor speed set at 1.8 rpm, the proportional controller gain set at 20, and the ground speed sampling rate set at 0.1 s, showed excellent performance for all sprayers with less than 1% of unacceptable area for each sprayer.

Variations in concentration were observable in the outer nozzles at a distance beyond the major application errors (figs. 11 through 16). These concentration variations resulted from differences in the chemical and carrier subsystem dynamics. They caused application errors that were much smaller than the errors due to the delays in the changes in the carrier flow rate that occurred at the first part of the simulation and were typically less than the recommended 5% error tolerance. The variation in concentration just downstream from the injection point was plotted as a function of distance for each of the baseline simulations run on the three sprayers (fig. 17). The maximum concentration variation for these three simulations was approximately 4.5% which is within the five percent error limit. Larger variation could be expected if greater differences in the response times of the chemical and carrier subsystems existed.

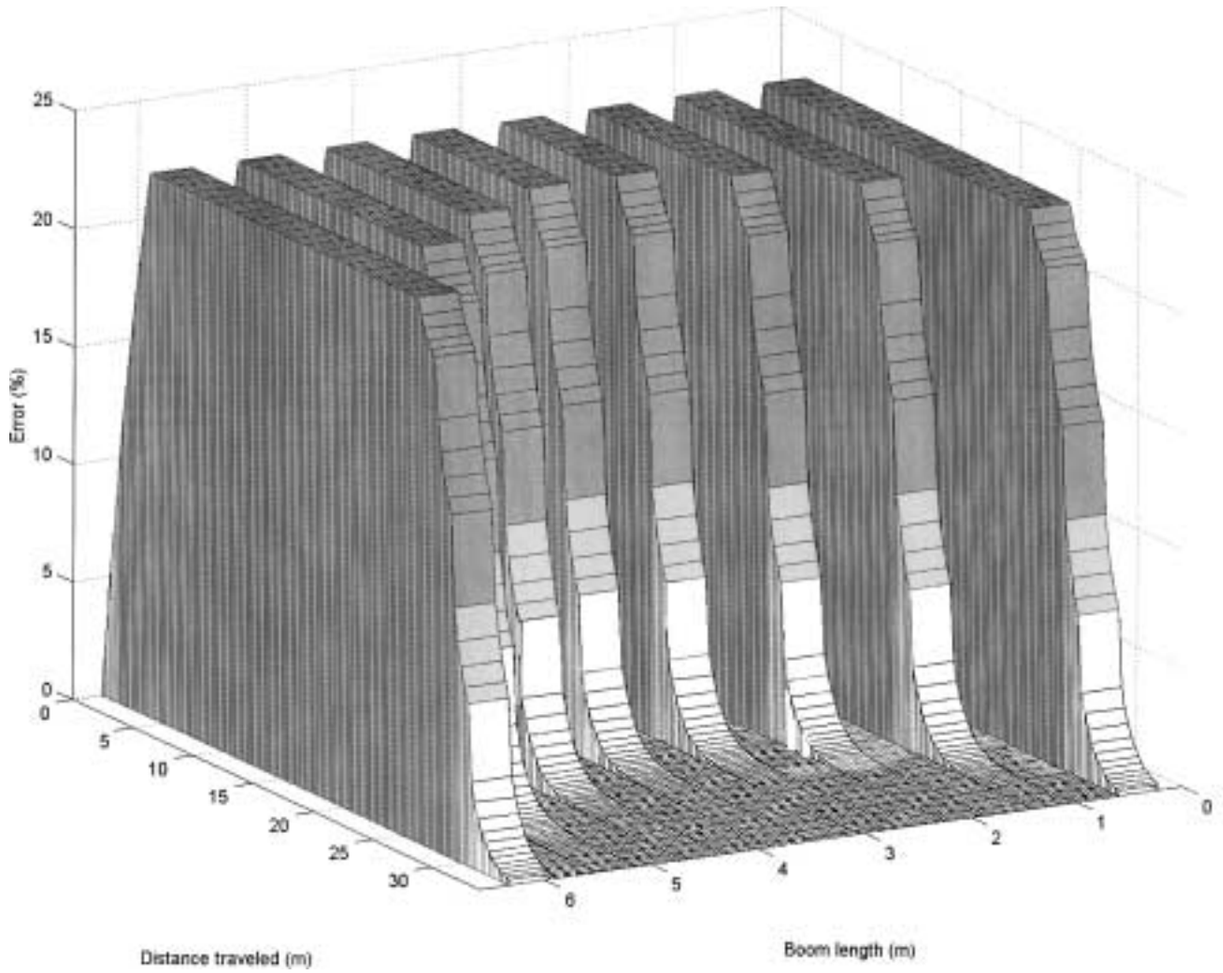

Figure 16–Application error versus distance traveled for the simulation of the private band sprayer without carrier control. White areas have less than 5% error. Gray areas have error between 5 and 10%. Dark gray areas have error greater than 10%.

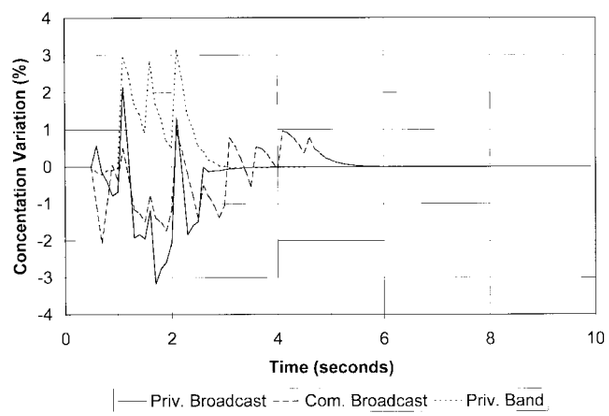

Figure 17–Concentration variation at injection point as a function of time for the baseline simulation of each sprayer with carrier control. Variation is a result of different dynamic response of the two control subsystems.

CONCLUSIONS

The sprayer simulation results provided evidence that chemical injection with carrier control will result in less application error than chemical injection without carrier control because carrier control minimizes the concentration variations to within dynamic response differences between the two subsystems, thus reducing the effect of transport delays. Nevertheless, the range of carrier control is limited to the workable pressure range of the nozzles. However, with the advent of modulated nozzles (Giles et al., 1996), potential exists for this range to be extended. In addition, these simulations provided evidence that further reductions in the application error produced by sprayers equipped with this type of control system is possible with increases in the rate at which ground speed data are available to the controller and the valve speed.

The dynamics of the carrier control subsystem are very much dependent on the actual components and physical configuration of particular sprayers. A limitation to the model developed of the carrier control system is that it is specific to the test system used. Nevertheless, the methodology used to generate the model is generally applicable to specific sprayer configurations.

The following specific conclusions were drawn:

1. The chemical control subsystem step response was predictable using the model developed in the project and was insensitive to head pressure.
2. The nonlinear model of the carrier hydraulics described the relationship between flow rate and valve element angle.
3. The voltage saturation effect in the carrier subsystem controller limited the speed of the valve motor, and, subsequently, the speed that changes could be made to the carrier flow rate. In addition, the speed at which flow rate measurements were available to the microprocessor limited how much the valve motor speed could be increased without creating instability.
4. The simulation results indicated that chemical injection with carrier control was a superior technique to simple chemical injection for applying chemicals when considering the problem of chemical concentration delay.
5. It was not necessary that the carrier subsystem controller have the exact same dynamics as the chemical subsystem controller. However, differences in the dynamics of these controllers should be minimized to reduce chemical concentration variations.
6. By increasing the ground speed sampling rate and speed of the carrier control valve motor, formulation application rate errors were reduced. Nevertheless, increases in valve motor speed led toward instability because of the large flow rate sampling interval.

ACKNOWLEDGMENTS. The authors would like to acknowledge Raven Industries for their support of this research.

REFERENCES

Ayers, P. D., S. M. Rogowski, and B. L. Kimble. 1990. An investigation of factors affecting sprayer control system performance. *Applied Engineering in Agriculture* 6(6): 701-706.

Aspelin, A. L. 1997. *Pesticide Industry Sales and Usage: 1994 and 1995 Market Estimates.* Washington, D.C.: U.S. Environmental Protection Agency, Office of Pesticide Programs.

Budwig, R. S., J. M. McDonald, and T. J. Karsky. 1988. Evaluation of chemical injection systems for mobile agricultural spray equipment. ASAE Paper No. 88-1592. St. Joseph, Mich.: ASAE.

Economic Research Service, USDA. 1997. Net value added and net farm income attains new highs in 1996. *Agricultural Income and Finance—Situation and Outlook Report.* AIS-66: 11.

_____. 1998. Total expenses for production inputs and services rose 5 percent in 1997. *Agricultural Income and Finance—Situation and Outlook Report.* AIS-69.

Franklin, G. F., J. D. Powell, and M. L. Workman. 1990. *Digital Control of Dynamic Systems.* Reading, Mass.: Addison-Wesley.

Gebhardt, M. R., C. L. Day, C. E. Goering, and L. E. Bode. 1974. Automatic sprayer control system. *Transactions of the ASAE* 17(6): 1043-1047.

Geiger, D. F. 1981. *Phase Lock Loops for DC Motor Speed Control.* New York, N.Y.: John Wiley & Sons.

Giles, D. K., G. W. Henderson, and K. Funk. 1996. Digital control of flow rate and spray droplet size from agricultural nozzles for precision chemical application. In *Precision Agriculture: Proc. 3rd Int. Conf. on Precision Agriculture*, eds. P. C. Roberts, R. H. Rust, and W. E. Larson, 729-738. Madison, Wis.: ASA/CSSA/SSSA.

Grisso, R. D., E. J. Hewett, E. C. Dickey, R. D. Schnieder, and E. W. Nelson. 1988. Calibration accuracy of pesticide application equipment. *Applied Engineering in Agriculture* 4(4): 310-315.

Karsky, T., R. Budwig, J. McDonald, and C. Quijano. 1990. Evaluation and development of chemical injection systems for mobile agricultural spray equipment. Final Report submitted to Western Region Pesticide Assessment Program, Davis, Calif.

Koo, Y. M., S. C. Young, and D. K. Kuhlman. 1987. Flow characteristics of injected concentrates in spray booms. ASAE Paper No. 87-1602. St. Joseph, Mich.: ASAE.

Larson, G. H., D. K. Kuhlman, and G. TenEyck. 1982. Direct metering of pesticide concentrations. ASAE Paper No. MC 82-134. St. Joseph, Mich.: ASAE.

Merritt, H. E. 1967. *Hydraulic Control Systems.* New York, N.Y.: John Wiley & Sons.

Ozkan, H. E. 1987. Sprayer performance evaluation with microcomputers. *Applied Engineering in Agriculture* 3(1): 36-41.

Peck, D. R., and L. O. Roth. 1975. Field sprayer induction system development and evaluation. ASAE Paper No. 75-1541. St. Joseph, Mich.: ASAE.

Raven Industries, Inc. 1987. *SCS-700 Installation and Service Manual.* Sioux Falls, S.Dak.

Reichard, D. L., and T. L. Ladd. 1983. Pesticide injection and transfer system for field sprayers. *Transactions of the ASAE* 26(3): 683-686.

Rider, A. R., and E. C. Dickey. 1982. Field evaluation of calibration accuracy for pesticide application equipment. *Transactions of the ASAE* 25(2): 258-260.

Spraying Systems Co. 1993. *Teejet® Agricultural Spray Product Catalog #43A.* Wheaton, Ill.: Spraying Systems Co.

Steward, B. L. 1994. Modeling and simulation of a chemical injection system. M.S. thesis. Brookings, S.Dak.: Hilton M. Biggs Library, South Dakota State University.

Sudduth, K. A., S. C. Borgelt, and J. Hou. 1995. Performance of a chemical injection sprayer system. *Applied Engineering in Agriculture* 11(3): 343-348.

Tompkins, F. D., K. D. Howard, C. R. Mote, and R. S. Freeland. 1990. Boom flow characteristics with direct chemical injection. *Transactions of the ASAE* 33(3): 737-743.

U.S. Department of Agriculture, U.S. Environmental Protection Agency. 1989. *Applying Pesticides Correctly, A Guide for Private and Commercial Applicators.* Washington, D.C.: GPO.

Vidrine, C. G., C. E. Goering, C. L. Day, M. R. Gebhardt, and D. B. Smith. 1975. A constant pesticide application rate sprayer model. *Transactions of the ASAE* 18(3): 439-443.

Way, T. R., K. Von Bargen, R. D. Grisso, and L. L. Bashford. 1992. Simulation of chemical application accuracy for injection sprayers. *Transactions of the ASAE* 35(4): 1141-1149.